Structures and superconducting properties of the high-pressure IV and V phases of calcium from first principles

Yansun Yao, John S. Tse, and Zhe Song
Department of Physics and Engineering Physics, University of Saskatchewan, Saskatoon, Saskatchewan, Canada S7N 5E2

Dennis D. Klug and Jian Sun
Steacie Institute for Molecular Sciences, National Research Council of Canada, Ottawa, Ontario, Canada K1A 0R6

Yvon Le Page
Institute for Chemical Process and Environmental Technology, National Research Council of Canada, Ottawa, Ontario, Canada K1A 0R6

(Received 19 October 2007; revised manuscript received 24 June 2008; published 11 August 2008)

Recently two high-pressure phases of Ca above 100 GPa have been identified and shown to possess high superconducting critical temperatures (T_c). Their crystal structures, however, are unknown. The search for low-enthalpy structures within the stability range using genetic algorithm and quasirandom methods yielded the same solutions. Both methods reveal a *Pnma* structure for Ca-IV and a *Cmca* structure for Ca-V. Calculated diffraction patterns are in substantial agreement with experiments. The proposed structures are both found to be superconducting, and the calculated T_c values are close to those observed for Ca-IV and Ca-V.

DOI: 10.1103/PhysRevB.78.054506 PACS number(s): 74.62.Fj, 63.20.K−, 74.25.Jb, 74.70.−b

I. INTRODUCTION

Superconductivity in elemental solids at high pressure is a subject of great importance and is relevant to the general area of enhanced electron-phonon coupling (EPC) in solids. Ca, being a "simple" metal, at high pressure was found to possess the highest superconducting critical temperature (T_c) of all elemental solids.[1] The T_c increases with pressure and reaches 25 K at 161 GPa, which is the highest observed T_c for all pressure-induced superconductors up to now.[1] At ambient pressure Ca has a face-centered-cubic (fcc) structure. Under high pressure it undergoes successive phase transitions into a body-centered-cubic (bcc) phase at 20 GPa then to a simple cubic (SC) phase at 32 GPa.[2] At higher pressures two forms have been identified:[3,4] Ca-IV near 100–110 GPa and Ca-V at about 139 GPa. The SC, Ca-IV, and Ca-V phases were all found to be superconducting.[1,5] The T_c increases linearly with pressure in the SC phase but less significantly in phases IV and V.[1] Knowledge of the lattice dynamics of these superconducting phases is necessary for understanding their electron-phonon mechanisms. However, the two high-pressure phases (Ca-IV and Ca-V) were found to coexist[5] over a wide pressure range, making their structures difficult to determine from experimental diffraction patterns due to overlapping Bragg peaks from these two phases. Moreover, the experimental diffraction patterns are also strongly interfered by the Bragg peaks from the gasket material used in the diamond-anvil cell.[5] Given these experimental difficulties, although the x-ray powder-diffraction patterns of Ca-IV and Ca-V have been reported,[5] the structural solution of these two high-pressure phases remains elusive.

In the present study, an extensive search for possible structures for Ca-IV and Ca-V was performed using two recently developed structure optimization techniques. Both methods succeeded and converged to the same solutions. Two energetically very competitive structures were found. Comparison between theoretical and observed diffraction patterns shows that Ca-IV, which is observed between 110–130 GPa, has a *Pnma* space group while the higher pressure Ca-V phase has a *Cmca* structure. Both phases are found to be superconducting and the predicted T_c are close to their respective observed values. The structure predicted for Ca-IV phase differs from a recent theoretical study that used metadynamics simulation.[6] It is shown here that the calculated diffraction pattern for the previously proposed $P4_3$ structure[6] for Ca-IV does not agree with the experiment. Moreover, this structure is energetically inferior to both the *Cmca* and *Pnma* structures at pressures higher than 110 GPa. Contrary to recent theoretical studies showing that a common feature for enhancing EPC in high-pressure solids is near the vicinity of electronic and structural instability,[7–9] it is perhaps surprising to find that EPCs of both Ca-IV and Ca V are distributed almost evenly over the first Brillouin zone (BZ).

II. METHODS AND COMPUTATIONAL DETAILS

The searches for low-enthalpy crystal structures were performed with recently proposed genetic algorithm (GA) (Refs. 10–14) and quasirandom methods.[15–18]

A. Genetic algorithm

GA calculations were performed using our own implementation of the methods described in Refs. 10–13, combining features from recently proposed strategies as well as several improvements.[14] The search procedure starts with a population of randomly generated structures. The population is improved through heredity, mutation, and retaining operations followed by *ab initio* structural optimizations to produce energetically favorable structures. In each successive

generation, new low-enthalpy structures evolve and replace the highest enthalpy structures in preceding generation. A structure analysis package has been implemented to examine structural similarity between structures in the population based on the comparison of the radial distribution functions (RDF) and the space group symmetries.[19] In the present study, structural searches were performed at 120 and 165 GPa starting with a population of 80 candidate structures with supercells containing eight randomly distributed Ca atoms. In the following, Z is defined as the number of atoms per primitive cell. In an eight-atom model structure, values of $Z=1$, 2, 4, and 8 can be derived from the processing of optimized structures. The genetic evolution cycle is repeated until no low-enthalpy structures were found in successive generations. It is found that 20 structural evolution generations was sufficient to achieve converged results for each pressure.

B. Quasirandom methods

The quasirandom search was performed with the low energy models obtained numerically (LEMON) tool within MATERIALS TOOLKIT.[15] An approximate value of the cell volume per formula unit (VFU), expected at that pressure, is first obtained by compression to the desired pressure of any reasonable model with that formula. The procedure then creates batches of random cells with volume Z^*VFU within axial ratio limits on the reduced cell imposed by the value of Z and the fact that the material here is expected to be metallic. Those cells are then filled up with atoms at random positions but with a minimum interatomic distance calculable from VFU. The models are then optimized via *ab initio* calculations. This is followed by a number (usually two) of *nudge* cycles[16] where the atomic positions and cell vectors are altered by vectors with same lengths in random directions on all partly optimized candidate structures; each nudge cycle is followed by *ab initio* optimization. LEMON batches of 999 initial structures were produced for each Z value ($Z=1$–12 atoms per primitive cell) at both 130 and 160 GPa. Optimized models from LEMON batches are then automatically sorted for identical structures in their reduced cells, forming usually about 20 groups of distinguishable optimized structure models per batch, which are ranked by enthalpy values. The procedure is entirely numerical and fully automated until a typical entry in the group with lowest enthalpy is examined for structure and symmetry.

C. Computational details

The structural optimization calculations in both GA and quasirandom methods were performed with the program VASP (Ref. 20), employing the projected augmented wave (PAW) pseudopotential included in the released pseudopotential library.[21] The Ca pseudopotentials employ $3p4s$ and $3s3p4s$ as valence states for GA and quasirandom methods, respectively, and no significant difference was found for the these two valence treatments. No symmetry was assumed in both structural search methods. The Monkhorst-Park (MP) meshes[22] were used for the first BZ sampling. In the GA calculations, the MP meshes were scaled according to the length of the reciprocal-lattice vectors of the candidate structure with a basic division of four, i.e., $4\times4\times4$ is the smallest mesh. In the quasirandom calculations, 512 k points were evenly distributed in the BZ and scaled according to length of the reciprocal-lattice vectors of the candidate structure.

Electronic band structure, phonon, and electron-phonon calculations were performed with the program package QUANTUM ESPRESSO (Ref. 23), employing the ultrasoft pseudopotentials[24] with nonlinear core corrections and $3p4s$ as valence states. This pseudopotential has been carefully examined by reproducing the experimental equations of states (EOSs).[25] The electronic wave function and the charge density were expanded with a kinetic-energy cutoff of 50 and 700 Ry, respectively. The electronic band structures were computed with a $16\times24\times24$ and $24\times24\times24$ MP k-point meshes for the *Pnma* (Ca-IV) and *Cmca* (Ca-V) phases, respectively. For the *Pnma* phase, individual phonon calculations were performed on a $4\times6\times6$ MP q-point mesh with a $8\times12\times12$ MP k-point mesh for the first BZ integrations. For the *Cmca* phase, individual phonon calculations were performed on a $6\times6\times6$ MP q-point mesh with a $12\times12\times12$ MP k-point mesh for the first BZ integrations. For the *Pnma* phase, the EPC has been calculated in the first BZ on a $4\times6\times6$ MP q-point mesh using individual EPC matrices obtained with a $16\times24\times24$ MP k-point mesh. For the *Cmca* phase, the EPC has been calculated in the first BZ on a $6\times6\times6$ MP q-point mesh using individual EPC matrices obtained with a $24\times24\times24$ MP k-point mesh. The geometry optimization and EOS for selected Ca polymorphs were calculated with the VASP code employing PAW $3s3p4s$ pseudopotential using a $16\times16\times16$ MP k-point set on the primitive cell. To examine the validity of the pseudopotential calculations, the full potential linearized augmented plane-wave (FLAPW) method implemented in WIEN2K code[26] was used to compute the total energy of the *Pnma* and *Cmca* structures at several selected pressure points. In these calculations, the generalized gradient approximation (GGA) (Perdew-Burke-Ernzerhof[27]) exchange-correlation functional was employed. For the *Cmca* structure, BZ integration was performed with 9792 k points in the irreducible wedge. For the *Pnma* structure, 9350 k points were used.

III. RESULTS AND DISCUSSIONS

A. Structures of Ca-IV and V

The GA and LEMON quasirandom methods each identified the same candidate structures at these pressures. LEMON batches where Z was 8 or 12 in the model resulted in supercells of the same low-enthalpy four-atom solutions. The agreement between the two very different structure prediction approaches can hardly be fortuitous. In addition, LEMON produced the same low-enthalpy results more than a hundred times at both pressures. In fact, the considerable redundancy of LEMON solutions constitutes a statistically strong indication that no other structures with lower or competitive enthalpies would likely exist at the pressures considered.

Two lowest enthalpy structures belonging to the space group *Pnma* and *Cmca* were found. Details of the predicted

TABLE I. Structural parameters for the predicted structures of Ca-IV and Ca-V, and a comparison of predicated and observed diffraction patterns for Ca-IV and Ca-V.

Phase	Pressure (GPa)	SG	Lattice parameters (Å)	Atomic coordinates fractional			
Ca-IV	120	*Pnma*	a=4.420 b=3.386 c=2.959	4*c*	0.326	0.250	0.614
Ca-V	140	*Cmca*	a=4.414 b=4.373 c=4.381	8*f*	0.000	0.169	0.685
			(derived from experiment)	2θ(exp) (deg)	Indices	2θ(cal) (deg)	
Ca-IV[a]	127	*Pnma*	a=4.560 b=3.227 c=3.040	13.45	101	14.08	
				16.12	011	16.11	
				19.17	210	19.17	
				19.54	201	19.57	
				22.15	020	22.15	
				22.50	212	22.52	
				23.53	002	23.54	
				25.13	102	24.83	
				26.14	121	26.35	
Ca-V[b]	139	*Cmca*	a=4.508 b=4.481 c=4.407	13.77	111	13.81	
				16.15	002	16.18	
				17.50	021	17.86	
				19.32	spurious (Ca-IV)		
				19.70	112	19.71	
				22.50	220	22.50	
				22.97	202	22.69	
				23.94	221	23.94	
				26.04	spurious (Ca-IV)		
				26.92	113	26.89	
				26.03	023	29.23	

[a]The calculated strong reflection 111 at 17.92° is hidden behind the Re gasket peak (see Fig. 1 in Ref. 3).
[b]The two spurious peaks are indexed to the Ca-IV phase.

structures are presented in Table I. The calculated enthalpy differences of the *Pnma* and *Cmca* structures with the Ca-III SC using the VASP code and PAW pseudopotential is shown in Fig. 1(a). The enthalpies of the two structures are more stable than the SC structure above 90 GPa (Ref. 28) and they are almost degenerate between 110–130 GPa. Above 130 GPa, the *Pnma* structure apparently is slightly more stable, however, the energy differences with the *Cmca* structure are insignificantly small. For example, at 140 GPa, the enthalpy of the *Cmca* structure is only 0.02 eV/atom (80 J/mol atom) higher than *Pnma*. Inclusion of zero-point energies increases the energy difference slightly to 0.026 eV/atom at 140 GPa. At the PAW optimized geometries, single point self-consistent calculations using meta-GGA (Refs. 30–32) were performed. The results give the same trend but the energy difference are now reduced almost by one order of magnitude. For example, at 140 GPa, the *Pnma* structure is more stable than the *Cmca* structure by only 0.0015 eV/atom. In view of the small energy differences and potential contribution of the core orbital to the total energy, calculations were repeated using an all-electron FLAPW method.[26] The trend of energy differences between the *Pnma* and *Cmca* phases is consistent with the VASP results. This small energy difference is beyond the limits of accuracy of the density-functional method. A small enthalpy difference indicates that these two phases may coexist over the pressure range from 110–140 GPa and the precise location of the Ca IV→V transition pressure will be difficult.

Based on the calculated enthalpies, it may be suggested that the *Cmca* and *Pnma* structures should correspond to the Ca-IV and Ca-V phases, respectively. A careful comparison of the calculated diffraction patterns, however, indicates otherwise. The calculated diffraction patterns for the *Cmca* and *Pnma* structures are compared with experiments in Fig. 1(b). It is obvious that the experimental diffraction patterns are much better reproduced with *Pnma* as Ca-IV and *Cmca* as Ca-V. As will be described below, detailed analysis of the crystallography of these two structures supports this assignment.

A recent theoretical study[6] on the high-pressure structures of Ca with metadynamics simulation starting from the SC structure of Ca-III also arrived at the same *Cmca* structure as Ca-V. However, using molecular-dynamics simulation, a $P4_3$ structure was proposed as a candidate for Ca-IV. To resolve

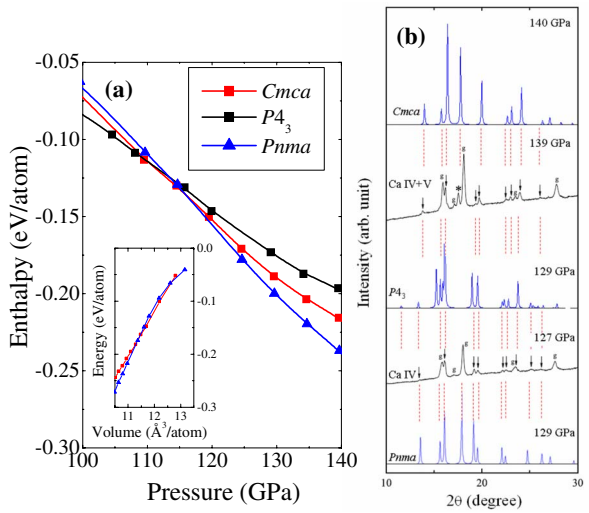

FIG. 1. (Color online) (a) Calculated enthalpies per atom as functions of pressure for three candidate structures *Pnma*, *Cmca*, and $P4_3$. The enthalpy of the SC phase is used as the zero-energy reference level. Inset: the energy-volume curves for these three structures. (b) Comparison of calculated and observed (black color) diffraction patterns for *Pnma*, *Cmca*, and $P4_3$ structures. The experimental diffraction patterns are taken from Ref. 3. The red lines are intended as guides to the eye for matching the theoretical and observed positions of the Bragg peaks.

this discrepancy, total-energy calculations with full geometry optimization using VASP, as described in the computation section, were performed on the $P4_3$ structure. The calculated enthalpies are compared with *Cmca* and *Pnma* structures in Fig. 1(a). The $P4_3$ structure is found to be more stable than the SC, *Cmca*, and *Pnma* structures only at pressures lower than 110 GPa. Both *Cmca* and *Pnma* become more stable when the pressure is over 110 GPa. Therefore the region of stability of the $P4_3$ structure is below the observed Ca-IV and Ca-V phases. More significantly, the calculated diffraction pattern of the $P4_3$ at 129 GPa [Fig. 1(b)] does not fit the experimental result for Ca-IV and it is not a viable candidate structure.

A comparison of the calculated diffraction patterns of the *Pnma* and *Cmca* structures with those reported for Ca-IV and Ca-V (Ref. 3) is given in Fig. 1(b). The experimental diffraction patterns for Ca-IV and Ca-V can be indexed successfully with the proposed structures. As shown in Table I, except for two spurious peaks that can be attributed to Ca-IV, all the experimental diffraction peaks can be indexed with the proposed *Cmca* structure of Ca-V. In particular, the diffraction peak observed at 17.86° in the experiment [shown in Fig. 1(b) with an asterisk], which was attributed in to the presence of phase V,[3] is correctly reproduced and is assigned to the strong 021 reflection. The unit-cell parameters derived from fitting the experimental pattern are very close to the theoretical predictions (Table I). The indexing for Ca-IV was not immediately obvious. Indices for calculated low-angle reflections of the proposed *Pnma* structure can be assigned unambiguously to the low-angle Bragg peaks (Table I). The recalculated cell parameters then index all the peaks with valid *Pnma* reflections. A strong reflection belonging to Ca-IV coincidentally overlaps with the gasket (marked *g*) at c.a. 18°.[3]

B. Structural relations between Ca-IV and Ca-V

The similarity of the diffraction patterns of the Ca-IV and Ca-V phases indicates that their structures may be closely related. Figures 2(a) and 2(b) depict the perspective view of the *Pnma* and *Cmca* structures, respectively. Both structures can be decomposed into stackings of 2D layers. The 2D planes are puckered in Ca-IV (*Pnma*) but become planar in Ca-V (*Cmca*). According to previous experience,[33] it is logical to expect a planar (2D) arrangement of the Ca atoms in the higher pressure structure. The structural motif of the 2D planes strongly resemble the 3^24^2 planar packing of regular polygons in 2D Archimedean tiling.[34] The 3^24^2 2D network has been observed in many high-pressure structures of the elemental solids—notably in the alkali metals,[33,35] such as the (110) plane of the *cI*16 phase of Li,[36] and the (010) plane of Rb-IV (Ref. 37) and Cs-III (Ref. 38). In the latter two cases, it has been shown that *s-d* mixing resulted in the localization of electron in the center of the "squares" of the 2D lattice.[33] Therefore, the observation of a similar 2D structural motif in the *Pnma* and *Cmca* structures is not unexpected. In fact, it adds credence to the validity of the predicted structures for Ca-IV and Ca-V. Figures 2(c) and 2(d) show the two structures in a common supercell, and illustrates the correspondence between the atom arrangements. The two structures have very similar primitive lattices. The *Pnma* cell corresponds to the $[\boldsymbol{c},(\boldsymbol{a}-\boldsymbol{b})/2,(\boldsymbol{a}+\boldsymbol{b})/2]$ primitive cell of the *C*-centered lattice of *Cmca* with cell angles of 93°, 90°, and 90°. In the phase transformation, the 93° cell angle reduces to 90°. As a consequence, new symmetry operations appear in the directions perpendicular to ***y*** and ***z*** in the *Pnma* structure. After the phase transformation, the ***n*** diagonal glide plane in *Pnma* structure becomes the ***a*** glide plane of the *Cmca* structure. The directions of the other two sets of planes of *Pnma* and *Cmca* structures are at about 45° from one another. This means that the phase transformation toggles the mutually perpendicular symmetry elements *ma* of the mirror plane *m* and glide plane reflection in the *a* direction from the *Pnma* structure [Fig. 2(c)] into the different mutually perpendicular elements *mc* with the glide plane in the *c* direction at 45° from them in *Cmca* structure [Fig. 2(d)] with no change in the topology of interatomic bonds. The two structures have common symmetry elements perpendicular to the ***x*** direction in the *Pnma* structure, which is the ***z*** direction in *Cmca* structure, but are not mutually related by a group-subgroup relationship. The two structures are different distortions in different orthorhombic subgroups of the same primitive cubic phase SC that is known to exist up to 109 GPa. The driving force for the unusual phase transformation has a slightly greater packing efficiency in *Cmca* that compensates for its slightly higher total energy, giving it lower enthalpy at higher pressure.

C. Electronic and phonon band structures

Figures 3(a) and 3(b) show the electronic band structures of the *Pnma* and *Cmca* phases calculated at 120 and 140

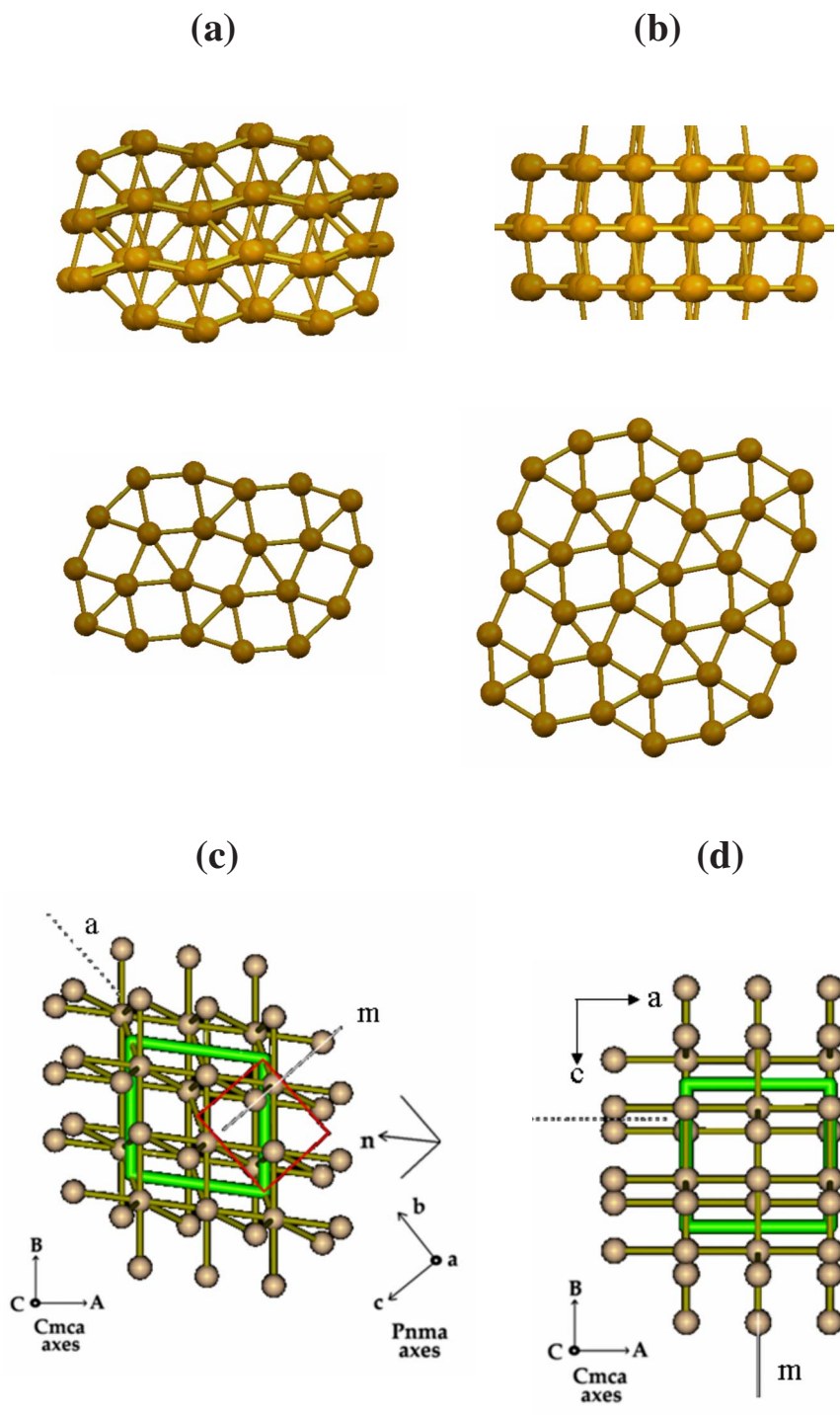

FIG. 2. (Color online) Perspective view of the crystal structure and a single layer of the 2D $3^2 4^2$ network for (a) Ca-IV (*Pnma*) and (b) Ca-V (*Cmca*). (c) and (d) show the crystal structures of the *Pnma* and *Cmca* phases in a common supercell.

GPa, respectively. For the *Cmca* band structure, an interesting feature is the occurrence of almost parallel bands crossing the Fermi level, e.g. along the $Y_2 \rightarrow T_2$, $Y_2 \rightarrow S$, and $R \rightarrow \Gamma$ lines. Parallel bands crossing the Fermi level are signs of possible nesting of two Fermi surfaces (FS). It was shown recently that the FS nesting tends to create hot zones in the first BZ enhancing EPC.[7,8] The phonon band structure of the *Pnma* and *Cmca* phases calculated at 120 and 140 GPa are depicted in Figs. 3(c) and 3(d). The absence of imaginary vibration modes shows that the *Pnma* and *Cmca* phases are stable. In *Cmca* Ca-V, Kohn anomalies[7,39] are observed in the optic branches halfway along $T_2 \rightarrow Z$ and $\Gamma \rightarrow Y_2$. Notable softening of acoustic phonons is found near Z in the $\Gamma \rightarrow Z$ direction, and near the T_2 and Y_2 symmetry points.

D. Electron-phonon coupling and superconductivity

To investigate the possibility of superconductivity, the phonon linewidths, EPC parameter λ, defined as the first reciprocal moment of the Eliashberg phonon spectral function $\alpha^2 F(\omega)$ was calculated using perturbative linear-response method within the density-functional approximation.[23] Figure 4 shows the spectral function $\alpha^2 F(\omega)$ and the integrated λ as functions of frequency for the

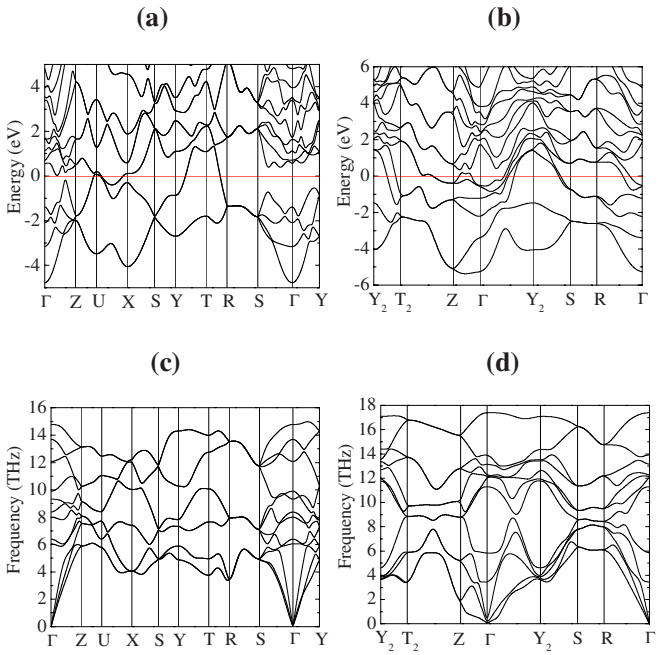

FIG. 3. (Color online) Calculated electronic band structure and phonon dispersion for the *Pnma* (a) and (c) at 120 GPa, and *Cmca* (b) and (d) at 140 GPa.

Pnma and *Cmca* structures calculated at 120 and 140 GPa, respectively. It is found that, in both the *Pnma* and *Cmca* phases, the EPC distribute almost evenly over the entire vibrational range. At 120 GPa, the calculated λ and phonon frequency logarithmic average $\omega_{\log}$ for the *Pnma* phase are 0.93 and 326 K, respectively. For the *Cmca* phase the calculated λ is 0.83 and $\omega_{\log}$ equals 341 K. At 140 GPa, the calculated λ and $\omega_{\log}$ for the *Pnma* phase are 0.85 and 351

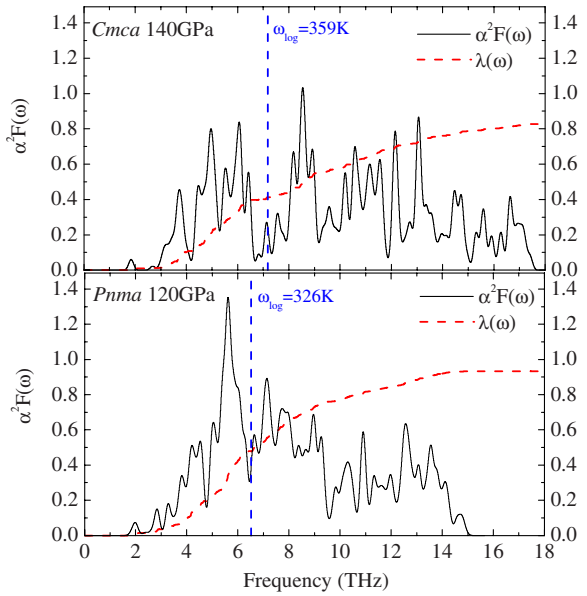

FIG. 4. (Color online) The Eliashberg phonon spectral function $\alpha^2F(\omega)$ and the electron-phonon integral $\lambda(\omega)$ of the *Cmca* phase at 140 GPa (top) and *Pnma* phase at 120 GPa (bottom). The phonon frequency logarithmic average $\omega_{\log}$ of each phase is marked.

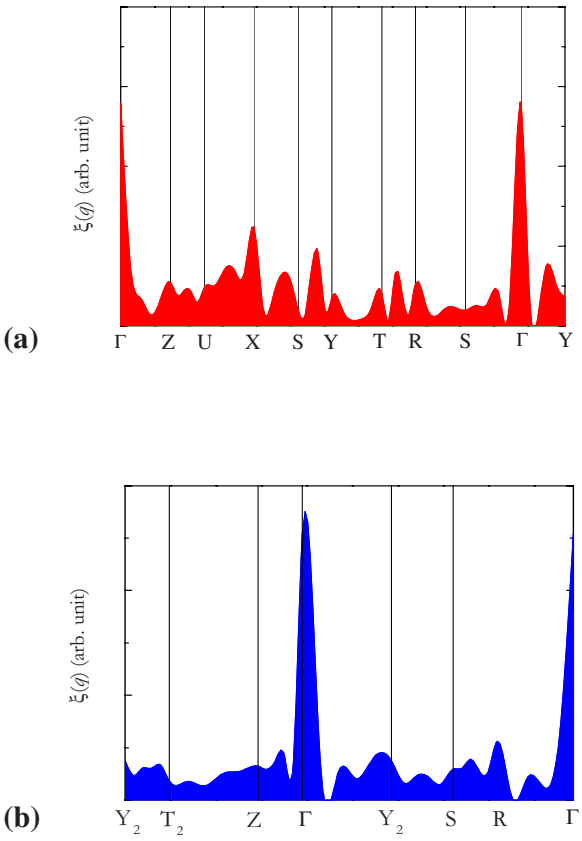

FIG. 5. (Color online) (a) The nesting function $\xi(q)$ along several high-symmetry lines of the first BZ for *Pnma* Ca at 120 GPa. (Note: the large peak at Γ is due to self-nesting and does not contribute to the electron-phonon coupling.) (b) The nesting function $\xi(q)$ along several high-symmetry lines of the first BZ for *Cmca* Ca at 140 GPa.

K, respectively, and the corresponding values for the *Cmca* phase are 0.84 and 361 K. The superconducting critical temperature T_c can be estimated from the Allen-Dynes modified McMillan equation,[40–42]

$$T_c = \frac{\omega_{\log}}{1.2}\exp\left[-\frac{1.04(1+\lambda)}{\lambda-\mu^*(1+0.62\lambda)}\right]. \quad (1)$$

Using an empirical value 0.1 for the Coulomb pseudopotential μ^*, the estimated T_c is 20 K for the *Pnma* phase and 17 K for the *Cmca* phase at 120 GPa, and 18K for the *Pnma* phase and 19K for the *Cmca* phase at 140 GPa. The theoretically predicted values are close to the recent experimentally observed T_c of 24.12 K at 120 GPa for Ca-IV and 20.5 K at 140 GPa for Ca-V.[1] To investigate the pressure dependence, T_c was calculated at 160 GPa for the *Cmca* phase. At 160 GPa, the λ increases to 0.92, $\omega_{\log}$ increases to 368 K, and the T_c is 22 K. This value is close to the experimental measured value of 25.7 K.[1] The calculated pressure coefficient (dT_c/dP) of 0.17 K/GPa correctly reproduces the trend but is slightly lower than the observed value of 0.26 K/GPa.[1]

To analyze the dynamical mechanism involve in the superconductivity of the *Pnma* and *Cmca* phases, we investi-

gated the Fermi surfaces of these two phases by studying the nesting function,[7]

$$\xi(q) = \frac{1}{N}\sum_k \delta(\varepsilon_k - \varepsilon_F)\delta(\varepsilon_{k+q} - \varepsilon_F) \propto \oint \frac{d\ell_k}{|\vec{v}_k \times \vec{v}_{k+q}|}, \quad (2)$$

where the line integral is evaluated along the intersection of Fermi surface and its image displaced by vector q, $\vec{v}_k$ is the Fermi velocity, and N the number of k points. The calculated nesting functions (*Pnma* at 120 GPa and *Cmca* at 140 GPa, respectively) are depicted in Fig. 5. The nesting functions of these two high-pressure phases of Ca are evenly distributed in the first BZ, indicating that there is no particular nesting (hot spots) dominating the EPC. This feature distinguishes high-pressure Ca from some other pressure-induced superconductors[7,8] that the EPCs are localized in the first BZ. On the other respect, as shown in Fig. 4, the EPCs of the *Pnma* and *Cmca* phases also show even distribution over the entire frequency range. There are no particular vibrational modes that dominate the total EPC.

The isotropic distribution of EPC in both coordinate and momentum spaces explains the good agreement between the calculated T_c with those observed in the experiments. For materials where the EPC is localized in very small regions of the first BZ, e.g., boron-doped diamond,[43] very dense k/q-point meshes are needed to reach proper convergence on the calculated EPC parameter λ. An approach[43,44] was proposed recently to sample the first BZ with millions of k points and then use the results to obtain the electron-phonon matrix at arbitrary electron-phonon momentum q. In the case of the *Pnma* and *Cmca* phases of Ca, since the EPCs are evenly distributed in the first BZ, this technique is not needed. The k/q-point meshes used in the present calculations should be adequate and the results are expected to be reliable.

IV. CONCLUSIONS

Using two structural search methods, two energetically almost degenerate structures with *Pnma* and *Cmca* space groups are found between 110–160 GPa. The energy difference between these two structures is very small so that it is difficult to make a clear identification of the calculated structures to the two phases of Ca based on the energetics. Through the comparison of calculated and observed diffraction patterns, it is shown that Ca-IV has the *Pnma* structure and Ca-V has the *Cmca* structure. Both structures are found to be superconducting. The superconductivity critical temperatures T_c have been calculated at three pressures: 120, 140, and 160 GPa. The calculated trend and predicted T_c agree well with experimental measurements. From the analysis of the Eliashberg spectral functions and nesting functions, the high T_c observed in these structures are attributed to a combination of fairly large λ and that almost all phonon modes contribute to the EPC processes leading to a large $\omega_{\log}$. The mechanism presented here differs from that of some other pressure-induced superconductors in which the superconductivity is associated with strong electronic and dynamical instability.[7,8] In view of the high T_c the simplicity of the electron-phonon coupling mechanism is surprising and raises the possibility that even higher T_c materials may be found at high pressure.

[1] T. Yabuuchi, T. Matsuoka, Y. Nakamoto, and K. Shimizu, J. Phys. Soc. Jpn. **75**, 083703 (2006).
[2] H. Olijnyk and W. B. Holzapfel, Phys. Lett. **100**, 191 (1984).
[3] T. Yabuuchi, Y. Nakamoto, K. Shimizu, and T. Kikegawa, J. Phys. Soc. Jpn. **74**, 2391 (2005).
[4] Y. Nakamoto, T. Yabuuchi, T. Matsuoka, K. Shimizu, and K. Takemura, J. Phys. Soc. Jpn. **76**, 25 (2007).
[5] S. Okada, K. Shimizu, T. C. Kobayashi, K. Amaya, and S. Endo, J. Phys. Soc. Jpn. **65**, 1924 (1996).
[6] T. Ishikawa, A. Ichikawa, H. Nagara, M. Geshi, K. Kusakabe, and N. Suzuki, Phys. Rev. B **77**, 020101(R) (2008).
[7] D. Kasinathan, J. Kuneš, A. Lazicki, H. Rosner, C. S. Yoo, R. T. Scalettar, and W. E. Pickett, Phys. Rev. Lett. **96**, 047004 (2006).
[8] J. S. Tse, Y. Yao, and K. Tanaka, Phys. Rev. Lett. **98**, 117004 (2007).
[9] Y. Yao and J. S. Tse, Phys. Rev. B **75**, 134104 (2007).
[10] D. M. Deaven and K. M. Ho, Phys. Rev. Lett. **75**, 288 (1995).
[11] A. R. Oganov and C. W. Glass, J. Chem. Phys. **124**, 244704 (2006).
[12] G. Trimarchi and A. Zunger, Phys. Rev. B **75**, 104113 (2007).
[13] N. L. Abraham and M. I. J. Probert, Phys. Rev. B **73**, 224104 (2006).
[14] Y. Yao, J. S. Tse, and K. Tanaka, Phys. Rev. B **77**, 052103 (2008).
[15] Y. Le Page and J. R. Rodgers, J. Appl. Crystallogr. **38**, 697 (2005).
[16] Y. Le Page and J. R. Rodgers, Comput. Mater. Sci. **37**, 537 (2006).
[17] C. J. Pickard and R. J. Needs, Phys. Rev. Lett. **97**, 045504 (2006).
[18] C. J. Pickard and R. J. Needs, Nat. Phys. **3**, 473 (2007).
[19] H. T. Stokes, D. M. Hatch, and B. J. Campbell (http://stokes.byu.edu/isotropy.html).
[20] G. Kresse and J. Furthmüller, Comput. Mater. Sci. **6**, 15 (1996).
[21] G. Kresse and D. Joubert, Phys. Rev. B **59**, 1758 (1999).
[22] H. J. Monkhorst and J. D. Park, Phys. Rev. B **13**, 5188 (1976).
[23] S. Baroni, S. de Gironcoli, A. Dal Corso, and P. Giannozzi, Rev. Mod. Phys. **73**, 515 (2001); http://www.pwscf.org
[24] D. Vanderbilt, Phys. Rev. B **41**, 7892 (1990).
[25] See EPAPS Document No. E-PRBMDO-78-008829 for auxiliary material to this article. For more information on EPAPS, see http://www.aip.org/pubservs/epaps.html.
[26] P. Blaha, K. Schwarz, G. K. H. Madsen, D. Kvasnicka, and J. Luitz, *WIEN2K, An Augmented Plane Wave Plus Local Orbitals Program for Calculating Crystal Properties* (Karlheinz Schwarz, Technische Universität Wien, Austria, 2002).
[27] J. P. Perdew, K. Burke, and M. Ernzerhof, Phys. Rev. Lett. **77**, 3865 (1996).

[28] In apparent contradiction to experimental observation, the SC phase was found to be unstable within the harmonic approximation using the computational techniques employed in this study. The result may indicate the SC structure is entropically stable or there is stronger anharmonicity for the interatomic interactions. In the latter case, it has been shown previously that, e.g., in $MgCNi_3$ (Ref. 29), phonon instability helps to enhance electron-phonon coupling.

[29] A. Y. Ignatov, S. Y. Savrasov, and T. A. Tyson, Phys. Rev. B **68**, 220504(R) (2003).

[30] S. K. Ghosh and R. G. Parr, Phys. Rev. A **34**, 785 (1986).

[31] A. D. Becke and M. R. Roussel, Phys. Rev. A **39**, 3761 (1989).

[32] J. Tao, J. P. Perdew, V. N. Staroverov, and G. E. Scuseria, Phys. Rev. Lett. **91**, 146401 (2003).

[33] J. S. Tse, Z. Kristallogr. **220**, 521 (2005).

[34] There are 11 different types of Archimedean tiling and each can be denoted by the symbol $(p_1^{q_1},p_1^{q_2},\cdots,p_s^{q_s})$, with $p_1,p_2,\ldots p_s$ denoting regular p-gons, and $q_1,q_2,\ldots q_s$ the number of adjacent regular p-gons of the same type that share the same vertex.

[35] J. S. Tse, Y. Yao, and Y. Ma, J. Phys.: Condens. Matter **19**, 425208 (2007).

[36] M. Hanfland, K. Syassen, N. E. Christensen, and D. L. Novikov, Nature (London) **408**, 174 (2000).

[37] R. J. Nelmes, M. I. McMahon, J. S. Loveday, and S. Rekhi, Phys. Rev. Lett. **88**, 155503 (2002).

[38] M. I. McMahon, R. J. Nelmes, and S. Rekhi, Phys. Rev. Lett. **87**, 255502 (2001).

[39] J. M. An, S. Y. Savrasov, H. Rosner, and W. E. Pickett, Phys. Rev. B **66**, 220502(R) (2002).

[40] P. B. Allen and R. C. Dynes, J. Phys. C **8**, L158 (1975).

[41] P. B. Allen and R. C. Dynes, Phys. Rev. B **12**, 905 (1975).

[42] W. L. McMillan, Phys. Rev. **167**, 331 (1968).

[43] F. Giustino, Jonathan R. Yates, I. Souza, M. L. Cohen, and S. G. Louie, Phys. Rev. Lett. **98**, 047005 (2007).

[44] F. Giustino, M. L. Cohen, and S. G. Louie, Phys. Rev. B **76**, 165108 (2007).